International Journal of Bridge Engineering (IJBE), Vol. 8, No. 3, (2020), pp. 75-86

STUDY OF SOLUTION CONVERGENCE FOR THE FINITE ELEMENT FOUR-NODE SHELL ELEMENT

Fathelrahman M. Adam[1], A.E. Mohamed[2],
Osama M. Elmardi Suleiman[3]

[1]Nile Valley University, Dept. of Civil Engineering, Sudan
[2]Sudan University of Science & Technology, School of Civil Engineering, Faculty of Engineering
[3]Nile Valley University, Dept. of Mechanical Engineering, Sudan
e-mail: fat470@yahoo.com, zobair1949@yahoo.com, osamamm64@gmail.com

ABSTRACT: This paper adopted a four-node degenerated shell element. A reduced integration point's scheme has been used as a remedy for the shear lock problem. The element was subjected to the patch test and passed all tests except the pure bending test. Different shell thicknesses have been adopted to find different ratios between thicknesses and the lengths of the elements for each mesh size. Some numerical examples have been applied, including curved and flat shells. Accordingly, different plots have been obtained by plotting the maximum displacements versus the ratios between the thicknesses and the lengths obtained of the elements for the different mesh sizes. The plots showed that the solution diverged after a certain value of the ratio which has been found equal to 0.23 for the curved shell and equal to 0.9 for the flat plate shell. These values were verified by using examples of known exact maximum displacement.

KEYWORDS: Shell Element, Degenerated Four-Nodes, Shear Lock, Membrane Lock, Reduced Integration.

1 GENERAL INTRODUCTION

The general concept of the finite element method is that the solution gained by it converges towards to the correct solution with increasing the mesh density. This concept is mostly, but not always, correct. Due to the assumptions accompanying the formulation of the method sometimes solution problems arise, especially in the application to thin shell elements, in which the problems of shear locking and membrane locking are encountered.

These problems often lead to the solution divergence. Although many solutions to these problems have been proposed and have been included in a large number of publications and have contributed to the solution of the problems in multiple applications, these problems still prevail in some different shell elements. Such special solutions were originally adopted in the linear case

by Ahmad et al. [l], Zienkiewicz et al [2], Hughes and Cohen [3] and had been subsequently used by many investigators. Other methods called Enhanced Assumed Strain (EAS) and Assumed Natural Strain (ANS) were also used to eliminate locking for the rectangular element, [4, and 5]. A technique of reduced and selective integration was also used which modifies the Gauss integration by combining both selective and weight modified integration [6, and 7]. A most effective method used to alleviate the shear locking is the Mixed Interpolation of Tensorial Components (MITC) method suggested by Dvorkin and Bathe [8] and lately modified to a new (MITC4+) shell element using a new assumed membrane strain field [9]. A solution had, also, been adopted by correcting the convergence curve to be asymptotic to the exact solution line by extrapolating the displacement using a Weibull model [7].

1.1 Aims and objective

This paper aims to solve the problem of shell finite element solution accompanied with the shear and membrane locking by presenting a linear formulation based on the four nodes degenerated shell finite element.

2 DEFINITION OF THE ELEMENT GEOMETRY

The four nodes degenerated shell finite element was presented by Kanock-Nukulchai [10]. The four nodes element shown in Figure 1 is obtained by degenerating the eight nodes solid element.

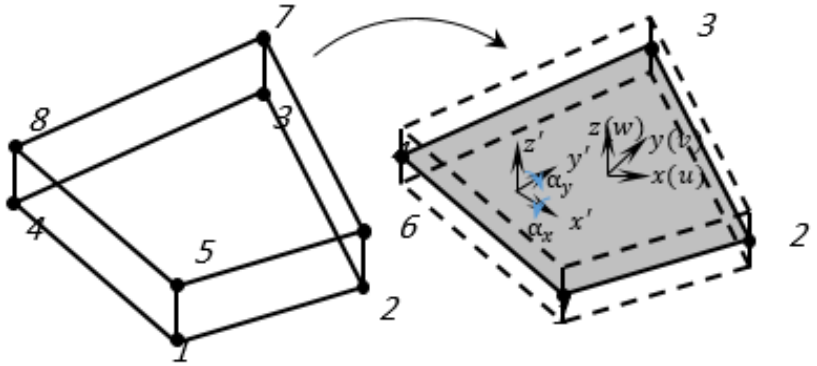

Figure 1. Degenerate four nodes shell element from eight nodes solid element

The shaded midsurface shown in Figure 1 is defined by natural coordinates (*r, s, t*). The displacements u, v and w are the displacements in global Cartesian coordinates *x, y* and *z* respectively. The rotations αx and αy are about local coordinates *x'* and *y'* respectively.

The shape functions for element at nodes are given by:

$$N_i (r, s) = ¼ (1 + r_i r) (1 + s_i s) \quad (1)$$

The thickness at node i, hi is computed normal to the midsurface, where i refers to the node number ($i = 1 – 4$).

The shell displacements field consists of the nodal displacements at midsurface u_i, v_i *and* w_i in global Cartesian coordinates *x, y* and *z* respectively in addition to the relative displacements produced by rotations α_{xi} *and* α_{yi} which are about local coordinates x' and y' respectively, as indicated in Figure 1. So, the general displacement variation can be expressed by:

$$\begin{Bmatrix} u \\ v \\ w \end{Bmatrix} = \sum_{i=1}^{4} N_i \begin{Bmatrix} u_i \\ v_i \\ w_i \end{Bmatrix} + \sum_{i=1}^{4} \tfrac{1}{2} th_i N_i \begin{bmatrix} l_{1i} & -l_{2i} \\ m_{1i} & -m_{2i} \\ n_{1i} & -n_{2i} \end{bmatrix} \begin{Bmatrix} \alpha_{yi} \\ \alpha_{xi} \end{Bmatrix} \quad (2)$$

where l_1, m_1 and n_1 (the direction cosines) are components of unit vector $\boldsymbol{v_1}$, and l_2, m_2 and n_2 are components of unit vector $\boldsymbol{v_2}$, where $\boldsymbol{v_1}$ and $\boldsymbol{v_2}$ are tangents to midsurface and are perpendicular to each other.

3 STRESSES AND STRAINS

The strains components along the local axes are given by Equation (3), assuming that the strain normal to midsurface $\varepsilon_{z'} = 0$.

By splitting Equation (3) into membrane component and shear component it can be rewritten as shown in Equations (4) and (5).

Hence, the matrices B_m, B_s can be derived by using Equation (6), where *T* is the transformation matrix.

$$\begin{Bmatrix} \varepsilon_{x'} \\ \varepsilon_{y'} \\ \gamma_{x'y'} \\ \gamma_{x'z'} \\ \gamma_{y'z'} \end{Bmatrix} = \begin{Bmatrix} \dfrac{\partial u'}{\partial x'} \\ \dfrac{\partial v'}{\partial y'} \\ \dfrac{\partial u'}{\partial y'} + \dfrac{\partial v'}{\partial x'} \\ \dfrac{\partial u'}{\partial z'} + \dfrac{\partial w'}{\partial x'} \\ \dfrac{\partial v'}{\partial z'} + \dfrac{\partial w'}{\partial y'} \end{Bmatrix} \quad (3)$$

$$\begin{Bmatrix} \varepsilon_{x'} \\ \varepsilon_{y'} \\ \gamma_{x'y'} \end{Bmatrix} = B_m \, u \quad (4)$$

$$\begin{Bmatrix} \gamma_{x'z'} \\ \gamma_{y'z'} \end{Bmatrix} = B_s \, u \quad (5)$$

$$\frac{\partial u', v', w'}{\partial x', y', z'} = T \frac{\partial u, v, w}{\partial x, y, z} \quad (6)$$

Assuming $\sigma_{z'} = 0$, the stress-strain relation can be stated as:

$$\begin{Bmatrix} \sigma_{x'} \\ \sigma_{y'} \\ \tau_{x'y'} \end{Bmatrix} = C_m \begin{Bmatrix} \varepsilon_{x'} \\ \varepsilon_{y'} \\ \gamma_{x'y'} \end{Bmatrix} \tag{7}$$

$$\begin{Bmatrix} \tau_{x'z'} \\ \tau_{y'z'} \end{Bmatrix} = C_s \begin{Bmatrix} \gamma_{x'z'} \\ \gamma_{y'z'} \end{Bmatrix} \tag{8}$$

Where C_m and C_s are the constitutive matrices for the membrane component and shear component respectively which are given as:

$$C_m = \frac{E}{1-\nu^2}\begin{bmatrix} 1 & \nu & 0 \\ \nu & 1 & 0 \\ 0 & 0 & \dfrac{1-\nu}{2} \end{bmatrix}, C_s = \frac{E\mu}{2(1+\nu)}\begin{bmatrix} 1 & 0 \\ 0 & 1 \end{bmatrix} \tag{9}$$

Where μ = 5/6 is a factor that accounts for the thickness-direction variation of transverse shear strain, E is the modulus of elasticity and ν is Poisson's ratio.

3.1 The element stiffness matrix

The stiffness matrix can be split into two matrices, membrane and bending effects and can be written as:

$$K_m = \int_{-1}^{1}\int\int B_m^T C_m B_m \det J \, dr \, ds \, dt \tag{10}$$

$$K_s = \int_{-1}^{1}\int\int B_s^T C_s B_s \det J \, dr \, ds \, dt \tag{11}$$

Where J is the Jacobian matrix.

Finite element computer programs were developed to include the theory presented previously. The programs were coded in standard **Compaq Visual FORTRAN Professional Edition 6.5.0**.

The element was tested to evaluate its reliability and performance in different mesh configurations. The elements were tested using a spread of patch tests. Besides the patch test, numerous numerical examples were conducted by using different element thicknesses.

4 THE PATCH TEST

The patch test had been performed to evaluate the elements ability to model constant strain. The test was performed for all strain components. The two normal strains were tested under both pure bending and pure membrane loads to assess their performance under both load conditions. The patch used in the tests is shown in Figure 2 and has been adopted from Reference [11] under applied load of *1000 N*.

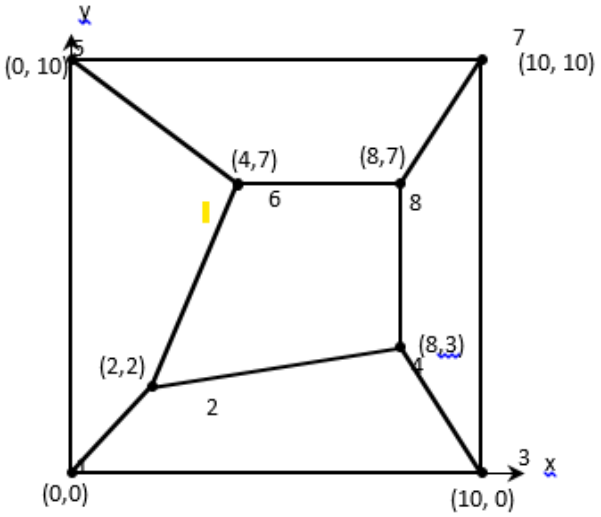

Figure 2. The patch test elements

The results obtained are summarized in Table (1). From the results it can be seen that all tests were passed except the test of pure bending.

5 NUMERICAL EXAMPLES

Five numerical examples which are widely used as bench marks are selected here.

Table 1. Summary of patch test results

Test / Stress	S_x	S_y	S_{xy}	S_{xz}	S_{yz}	State
Pure Bending x	758	382	-12	-6267	-6225	Not Passed
Pure In plane Shear	0	0	200	0	0	Passed
Pure Membrane x	200	0	0	0	0	Passed
Pure Transverse Shear xz	0	0	0	200	0	Passed

Note: The exact results for all test are equal to 200 N/mm^2 except for pure bending which is 1200 N/mm^2

The results have been presented in the form of plots of the maximum displacement versus the calculated ratio of the element thickness to its length for each mesh size. For the cylindrical shell, the length along the curved part has been used.

5.1 Pinched cylindrical shell

In this example, many values of thicknesses ranging between *2.75 mm* and *3.5 mm* have been used. The necessary data are shown in Figure 3.

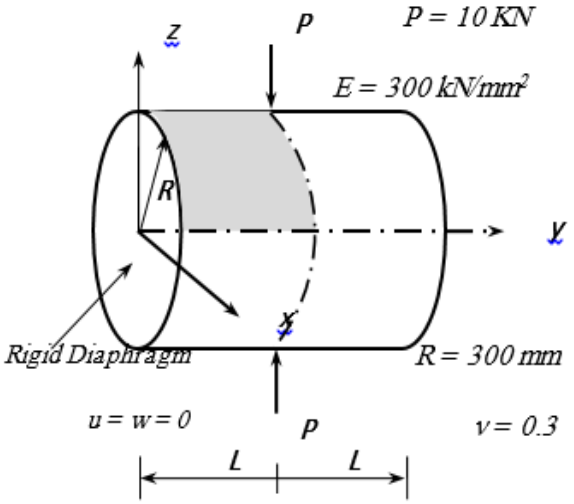

Figure 3. Pinched cylindrical shell

The results obtained for this example are shown in Figure 4.

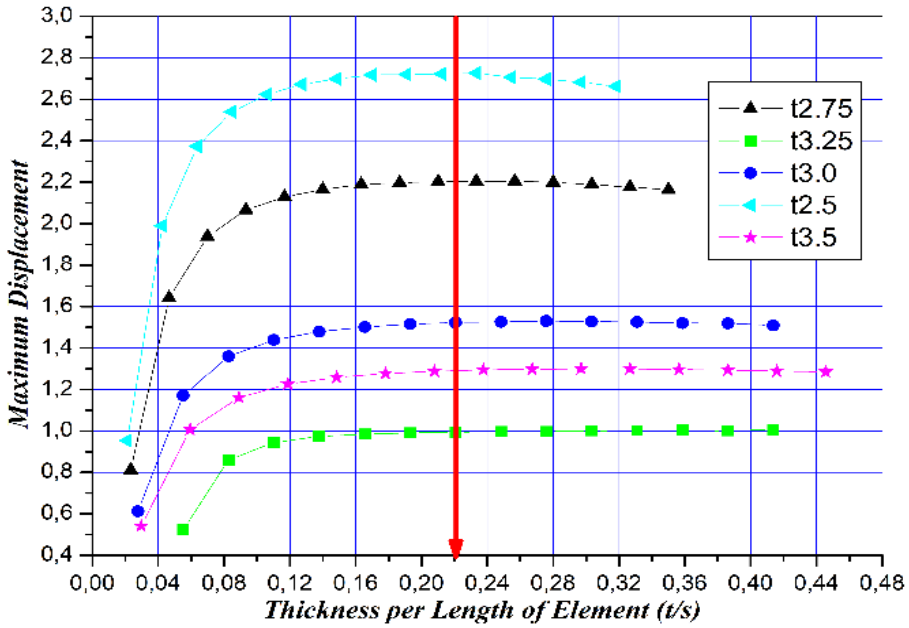

Figure 4. Results of pinched cylindrical shell example

5.2 Barrel vault (scordelis-lo roof)

In this example, the values of thicknesses are in the range from *0.25 ft* to *0.35 ft*. The data concerning this example are shown in Figure 5.

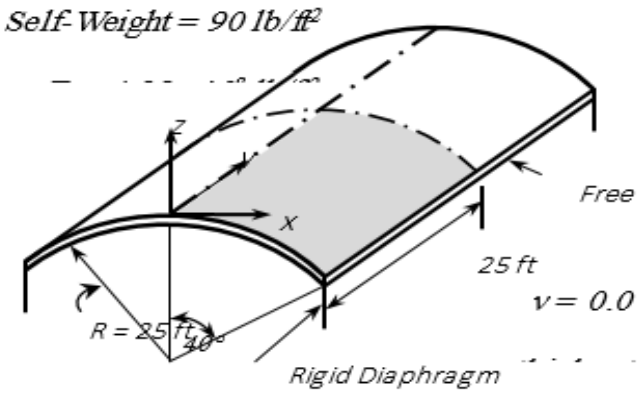

Figure 5. Scordelis-Lo roof

The results obtained for this example are shown in Figure 6.

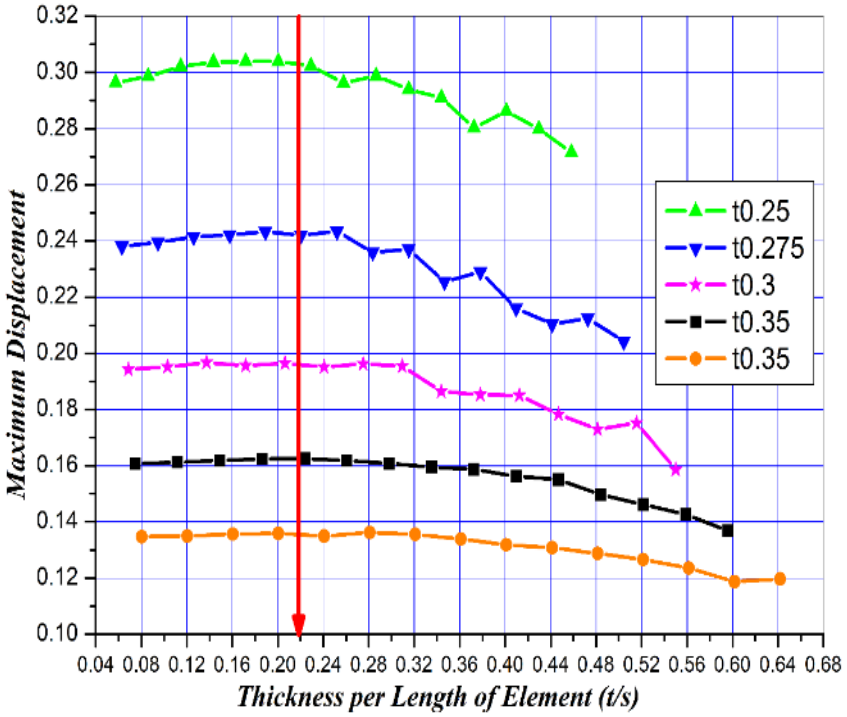

Figure 6. Results of Scordelis-Lo roof shell example

5.3 Simply supported thin plates

In this example, the values of thicknesses are in the range from *11 cm* to *12 cm*. The data concerning this example are shown in Figure 7**.** The results obtained for this example are shown in Figure 8.

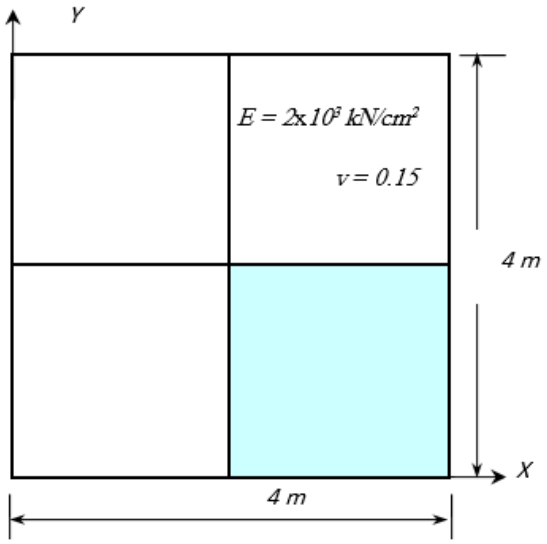

Figure 7. Simply supported thin plate example

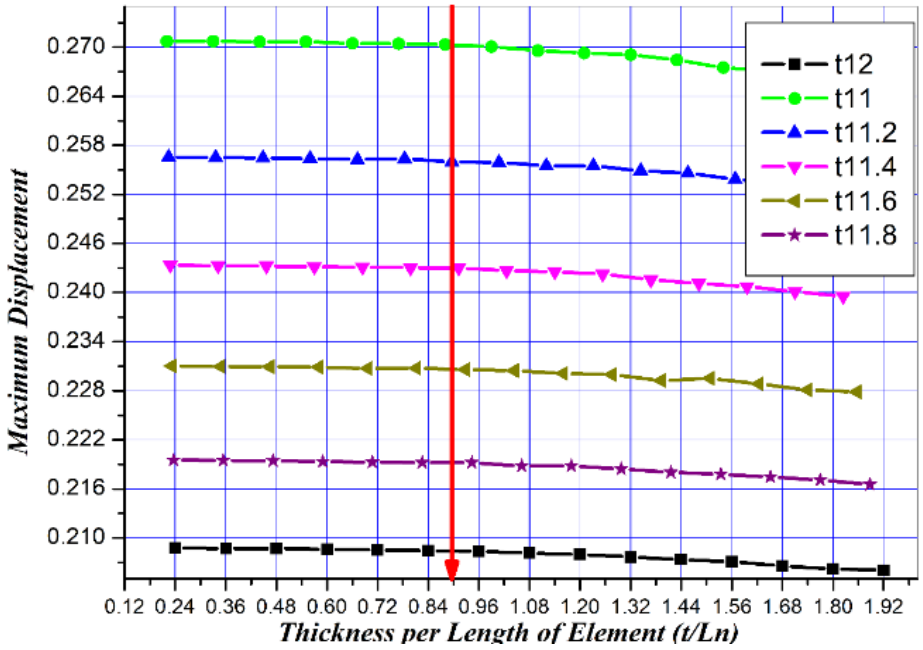

Figure 8. Results of simply supported thin plate example

5.4 Short cantilever beam

In this example, the values of thicknesses are in the range from *1.0 in* to *1.4 in*. The data concerning this example are shown in Figure 9

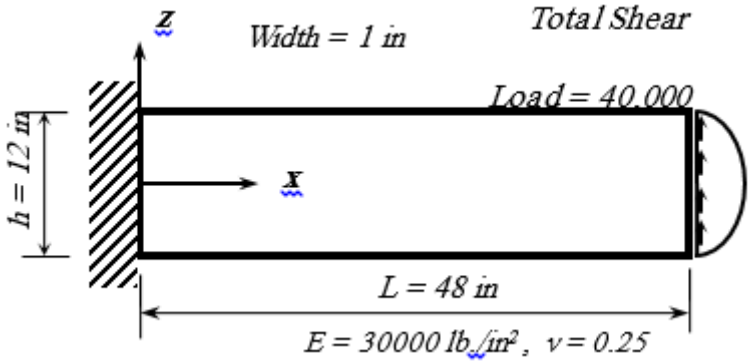

Figure 9. Short cantilever beam example

The results obtained for this example are shown in Figure 10.

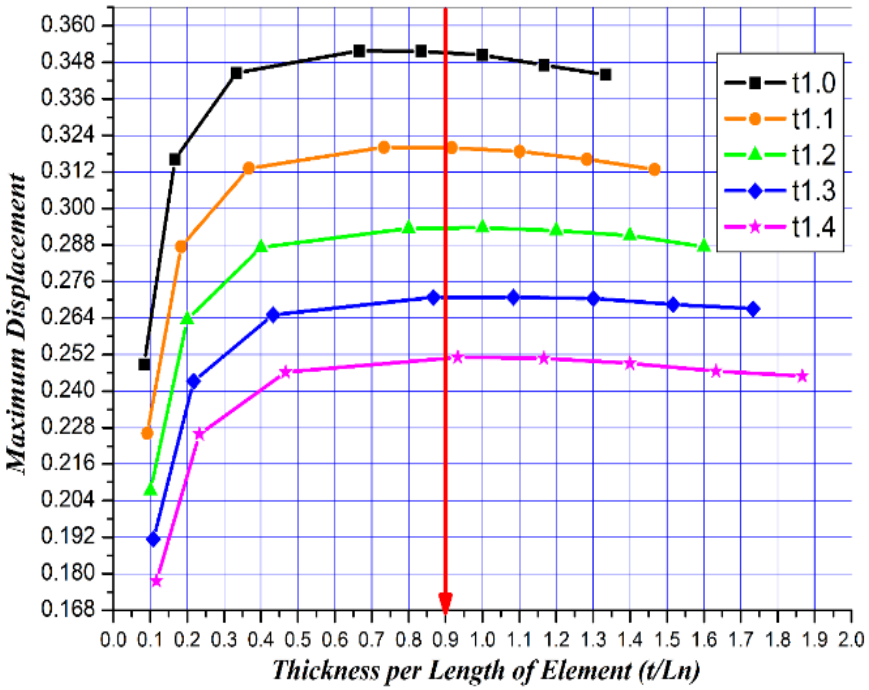

Figure 10. Results of short cantilever beam exam

6 DISCUSSION OF THE RESULTS

The length of the element segment for each mesh size (s) for the cylindrical shell and (L_n) for the flat plate shell, can be calculated from:

$$s = \frac{R\theta}{NEM} \quad \text{or} \quad L_n = \frac{L}{NEM} \tag{12}$$

Where R is the radius for the curved side, θ is the subtended angle and *NEM* is the number of elements for each mesh size.

As can be seen from Figures 4 and 6 which are related to the cylindrical shell, the convergence rate goes logically, but at a certain point, the divergence started and this matter is repeated for the different thicknesses of the shell. From observation, the ratio at which the divergence started to occur for the two examples is estimated by a value of 0.23 as indicated by the red arrow in the figures. Also, for the flat plate shell, the ratio at which divergence started to occur is estimated by a value of 0.9. These values of ratios can be used to calculate the suitable mesh size that give the best results close to the exact value. Accordingly, these values have been verified by using the following examples.

7 VERIFICATION OF THE SELECTED RATIOS

Three problems of known exact results have been used to verify the selected ratios for the two types of shells. The mesh size used is calculated according to the value of the ratio either 0.23 for curved shell or 0.9 for flat plate shell.

7.1 Pinched cylindrical shell

Same as the previous one shown in Figure 3 but with different data: (*P = 20 KN, E = 300 kN/mm^2, L = 1500 mm, R = 500 mm, v = 0.3, t = 5 mm*).

The exact maximum displacement under pinned load is *2.69693 mm*, was given by [12].

On-eight of the shell was analyzed so, the subtended angle θ is equal to *90º (1.571 in radian).* With using the ratio equal to *0.23*, the *s* can be calculated as:

$$s = \frac{t}{0.23} = \frac{5}{0.23} = 21.739$$

From Equation 12, the number of elements of mesh size can be calculated as

$$NEM = \frac{500(1.571)}{21.739} = 36.13$$

This means that the suitable mesh size that can be used is 36x36. The maximum displacement under pinned load obtained using this mesh size is *2.69087 mm*, which is almost identical (99.8%) to the exact result.

7.2 Spherical hinged cap

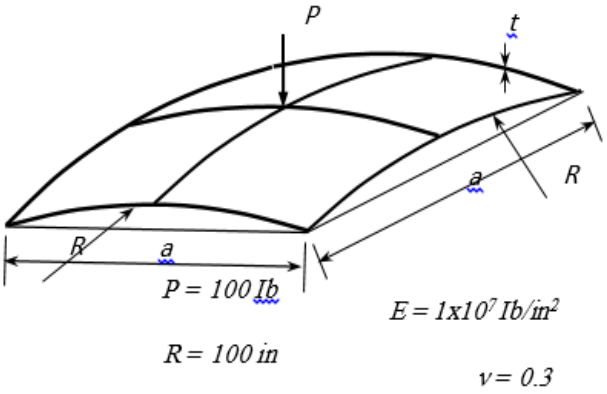

Figure 11. Spherical hinged cap

The exact maximum displacement under pinned load is *0.03956 in* as given by [13]. By the same procedure using ratio of 0.23, the suitable mesh size is found to be 37x37, which gives maximum displacement under pinned load of *0.03920 in*, which is almost identical (99.1%) with the exact one.

7.3 Simply supported thin plate

Same as the previous one shown in Figure 7 but with different data: (*Load* = $12x10^{-4}$ *kN/cm*^{2}, *E* = $2x10^3$ *kN/cm*^{2}, *L = 600 cm, v = 0.15, t = 15 cm*).

The exact maximum displacement at mid-point of the plate is *1.37157 cm* as given by [14]. Because of flat plate shell used here, the ratio taken is 0.9 and the corresponding mesh size has been found to be 18x18. This gives a maximum displacement of *1.37613 cm*, which is identical (100.3 %) with the exact one.

8 CONCLUSIONS

A four-node degenerated shell finite element was used by adopting five degrees of freedom per node. From the numerous methods recommended to use for solving the problem of locking, a reduced integration point's scheme was used. This remedy didn't solve the problem totally, still, the solution gained at certain mesh size tends to diverge with increased mesh size. The paper focused on this problem to obtain the mesh size at which divergence started to occur by using the ratio of thickness to the length of the element for each mesh size considered. This ratio is then used to calculate the suitable mesh size. The study focused on two types of shell: curved shell and flat plate shell. The ratios at which divergence started to occur have been found to be 0.23 for the curved shell and 0.9 for the flat plate shell. These ratios were verified using problems of known values of displacements. By comparing the results obtained using the mesh size which matches the ratio recommended, identical results were obtained (by a

ratio 99.1% to 100.3%) for the two types of shell. Finally, it is concluded that these ratios are reasonable to use for calculating the mesh size that will give acceptable results as general.

REFERENCES

[1] Ahmad S., Irons B.M. and Zienkiewicz O.C., "Analysis of thick and thin shell structures by curved finite elements", Internat. J. Numer. Meths. Engrg. 2, 419-451, 1970.
[2] Zienkiewicz C., Taylor R. L. and TOO I. M. "Reduced Integration Technique in General Analysis of plates and Shells", International Journal for Numerical Methods in Engineering, VOL. 3, 275-290, 1971
[3] Hughes T.J.R. and Cohen M., "The 'heterosis' finite element for plate bending", Computers and Structures, 9, 445-450, 1978.
[4] Huang H. C., "Implementation of assumed strain degenerated shell elements", Computers and Structures, vol. 25, no. 1, pp. 147–155, 1987.
[5] Marco Schwarze, and Stefanie Reese, "A reduced integration solid-shell finite element based on the EAS and the ANS concept-Large deformation problems", Int. J. Numer. Meth. Engng, **85**, 289–329, 2011.
[6] Kwon Y. D., Goo N. S., and Lim B. S., "Resolution of defects in degenerated shell elements through modification of Gauss integration," International Journal of Modern Physics B, vol. 17, no. 8-9, pp. 1877–1883, 2003.
[7] Fathelrahman M. Adam, Mohamed A. E., "Finite Element Analysis of Shell structures", LAP LAMBERT Academic Publishing, 2013.
[8] Bathe, K.J. and Dvorkin, E.N., "A formulation of general shell elements-the use of mixed interpolation of tensorial components", International Journal for Numerical Methods in Engineering ", Vol. 22, No. 3, pp. 697-722, 1986
[9] Yeongbin Ko, Phill-Seung Lee and Klaus-Jürgen Bathe, "A new MITC4+ shell element", Computers and Structures 182, 404–418, 2017
[10] Fathelrahman. M. Adam, Abdelrahman. E. Mohamed, A. E. Hassaballa, "Degenerated Four Nodes Shell Element with Drilling Degree of Freedom", IOSR Journal of Engineering (IOSRJEN), Vol. 3, Issue , PP 10-208, August. 2013
[11] Dvorkin E. N., "On Nonlinear Finite Element Analysis of Shell Structures", Ph.D. Thesis, Massachusetts Institute of Technology, 1984.
[12] John T. Perkins John T. Perkins, "ANALYTICAL STRIP METHOD FOR THIN CYLINDRICAL SHELLS", Ph.D. Thesis, University of Kentucky, 2017
[13] Ye T. Q., and Yuerang Zhao, "Quadrilateral Coons Surface Shell Finite Element with Discrete Principal Curvature Lines", Congr Int Counc Aeronaut Sci, Volume16, Issue 1, page 631-637, 1988.
[14] Lanheng Jin, "Analysis and Evaluation of a Shell Finite Element with Drilling Degree of Freedom", M.Sc. Thesis, University of Maryland at College Park, 1994.